Nuf, a Rab11 effector, maintains cytokinetic furrow integrity by promoting local actin polymerization

Jian Cao,[1] Roger Albertson,[1] Blake Riggs,[1] Christine M. Field,[2] and William Sullivan[1]

[1]Sinsheimer Laboratories, Department of Molecular, Cellular, and Developmental Biology, University of California, Santa Cruz, Santa Cruz, CA 95064
[2]Department of Systems Biology, Harvard Medical School, Boston, MA 02115

Plasma membrane ingression during cytokinesis involves both actin remodeling and vesicle-mediated membrane addition. Vesicle-based membrane delivery from the recycling endosome (RE) has an essential but ill-defined involvement in cytokinesis. In the *Drosophila melanogaster* early embryo, Nuf (Nuclear fallout), a Rab11 effector which is essential for RE function, is required for F-actin and membrane integrity during furrow ingression. We find that in *nuf* mutant embryos, an initial loss of F-actin at the furrow is followed by loss of the associated furrow membrane. Wild-type embryos treated with Latrunculin A or Rho inhibitor display similar defects. Drug- or Rho-GTP–induced increase of actin polymerization or genetically mediated decrease of actin depolymerization suppresses the *nuf* mutant F-actin and membrane defects. We also find that RhoGEF2 does not properly localize at the furrow in *nuf* mutant embryos and that RhoGEF2–Rho1 pathway components show strong specific genetic interactions with Nuf. We propose a model in which RE-derived vesicles promote furrow integrity by regulating the rate of actin polymerization through the RhoGEF2–Rho1 pathway.

Introduction

Cytokinesis, the physical separation of daughter cells after mitotic exit, requires the assembly of an actomyosin-based contractile ring that drives plasma membrane constriction and furrow ingression. The contractile ring forms perpendicular and midway to the anaphase spindle. Once the contractile ring forms, ingression of the cleavage furrow begins. Ingression of the animal cleavage furrow involves vesicle-mediated membrane addition as well as actomyosin-based contraction (Albertson et al., 2005; D'Avino et al., 2005; Glotzer, 2005). Thus, successful cytokinesis requires precise coordination between contraction and membrane addition.

Vesicle-based membrane delivery from both the Golgi and the recycling endosome (RE) is necessary for furrow ingression during cytokinesis (Lecuit and Wieschaus, 2000; Sisson et al., 2000; Skop et al., 2001, 2004; Xu et al., 2002; Farkas et al., 2003; Pelissier et al., 2003; Riggs et al., 2003; Fielding et al., 2005; Wilson et al., 2005; Giansanti et al., 2007). The RE, which is often found closely associated with microtubules, mediates vesicle transport directly to the plasma membrane (Ullrich et al., 1996). These properties make it especially well suited for regulating vesicle-mediated delivery to the cytokinesis furrows. Functional studies demonstrating a role for the RE in cytokinesis have relied extensively on *rab11* mutants. Rab11 is a small GTPase that preferentially localizes to the RE and is required for proper RE formation (Maxfield and McGraw, 2004). Consequently, *rab11* mutants render the RE nonfunctional and disrupt vesicle recycling to the plasma membrane. Mutations of *rab11* in *Caenorhabditis elegans*, *Drosophila melanogaster*, and mammalian cells all result in a failure to complete cleavage furrow ingression (Skop et al., 2001; Pelissier et al., 2003; Riggs et al., 2003; Wilson et al., 2005; Giansanti et al., 2007).

Additional support for a specific role of the RE in vesicle-mediated membrane delivery during cytokinesis comes from analysis of the Rab11 effector protein Nuf/FIP3/Arfophilin2. Genetic studies in *D. melanogaster* identified the centrosome-associated protein Nuf (Nuclear-fallout) as being essential for proper furrow formation in the early embryo (Sullivan et al., 1993; Rothwell et al., 1998; Riggs et al., 2003). Nuf is a homologue of mammalian FIP3/Arfophilin2 and both share a conserved 20-aa C-terminal Rab11 binding domain (Hickson et al., 2003; Riggs et al., 2003). GST pulldowns demonstrate that Nuf

Correspondence to William Sullivan: sullivan@biology.ucsc.edu
Abbreviations used in this paper: RE, recycling endosome; WT, wild type.
The online version of this paper contains supplemental material.

The Rockefeller University Press $30.00
J. Cell Biol. Vol. 182 No. 2 301–313
www.jcb.org/cgi/doi/10.1083/jcb.200712036

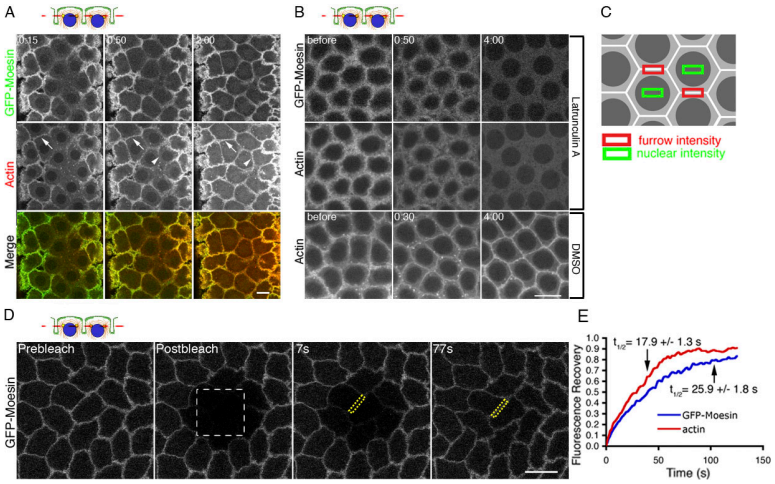

Figure 1. **F-actin is rapidly turned over in the furrow through depolymerization and repolymerization.** The schematic illustrates the focal plane relative to the furrow. Blue, nuclei; green, membrane. (A) Rhodamine-actin (red) was rapidly incorporated into preexisting (arrows) and newly forming (arrowheads) furrows marked by GFP-Moesin (green) at cycle-12 prophase. (B) GFP-Moesin and Rhodamine-actin showed a dramatic signal decrease at the furrow within 4 min after LatA but not DMSO injection. (C) Areas measured to calculate net furrow intensity (furrow intensity – nuclear intensity). (D and E) FRAP analysis of actin turnover during cycle-13 prophase. (D) White box indicates photobleached area. Yellow boxes indicate an example of a furrow region used for quantifications in E. See Video 1 (available at http://www.jcb.org/cgi/content/full/jcb.200712036/DC1). (E) Relative fluorescence intensities of GFP-Moesin and Rhodamine-actin at the furrows (y axis) after photobleaching (from D; *n* = 10 embryos). Bars, 10 µm.

and Rab11 physically associate and functional studies demonstrate that Nuf and Rab11 are mutually required for their localization to the RE (Riggs et al., 2003).

Mutational analysis reveals that Nuf and Rab11 are involved in proper membrane and actin organization at the invaginating furrows (Rothwell et al., 1998, 1999; Riggs et al., 2003). In *nuf* embryos, regions of the furrow are devoid of F-actin but not of other core furrow components (Rothwell et al., 1998). In addition, extensive gaps in the membrane are observed in the furrows of *nuf* and *rab11* embryos (Rothwell et al., 1999; Riggs et al., 2003). Associated with these gaps is an extensive accumulation of vesicles in the cortex, suggesting that these mutations disrupt RE-based vesicle-mediated delivery to the invaginating furrows (Rothwell et al., 1999; Riggs et al., 2003).

The fact that disrupting RE function through the *nuf* and *rab11* mutants produces defects in both membrane and F-actin organization suggests that these processes are closely linked (Riggs et al., 2003). To explore this linkage, we examined the relationship between F-actin turnover and stability of the metaphase and cellularization furrows in the early *D. melanogaster* embryo. Although actin turnover at the cytokinetic furrow has been well documented in other systems (Pelham and Chang, 2002; Guha et al., 2005; Murthy and Wadsworth, 2005), the functional significance remains unclear and the relationship between turnover and membrane stability has not been specifically explored. An advantage of studying this issue in the early *D. melanogaster* embryo is that furrow formation does not rely on actomyosin-based contraction (Royou et al., 2004). Surprisingly, disrupting myosin II function through mutations, antibody injection, or small molecule inhibitors has little effect on furrow progression (Royou et al., 2004). The same experiments performed in tissue culture cells undergoing conventional cytokinesis produced profound disruptions in furrow progression (Somma et al., 2002; Echard et al., 2004; Eggert et al., 2004). Furrow invagination in the early *D. melanogaster* embryos is driven primarily by vesicle-mediated membrane addition (Lecuit and Wieschaus, 2000; Sisson et al., 2000; Pelissier et al., 2003; Riggs et al., 2003). This enables us to explore functions of F-actin turnover that are independent of its role in actomyosin-based contraction.

In this paper, we describe a set of experiments that demonstrate that F-actin is required for the stability of the furrow membrane and actin turnover is required for normal furrow elongation. We also propose a model in which Nuf, a Rab11 effector, regulates furrow maintenance by regulating the rate of F-actin polymerization through the RhoGEF2–Rho1 pathway.

Results

F-actin is rapidly turned over at the furrow through depolymerization and repolymerization

To investigate actin dynamics at the metaphase furrows, we injected Rhodamine-labeled monomeric actin into embryos expressing the F-actin–specific label GFP-Moesin. The specificity for F-actin labeling (Edwards et al., 1997) was confirmed by colocalization of GFP-Moesin with phalloidin staining (Fig. S1, available at http://www.jcb.org/cgi/content/full/jcb.200712036/DC1). Monomeric Rhodamine actin was incorporated into newly forming furrow tips (Fig. 1 A, arrowheads). Interestingly, within 15 s after injection, Rhodamine-actin was rapidly incorporated into preexisting furrows and its fluorescence continued to increase for at least 2 min after injection (Fig. 1 A, arrows). The observation that actin polymerization occurred within existing cytokinetic furrows reveals that furrows are dynamic rather than static structures.

To determine whether furrow actin undergoes both polymerization and depolymerization, we used LatA (Latrunculin A), a small molecule that inhibits actin polymerization by sequestering actin monomers. LatA was injected into GFP-Moesin–expressing embryos during furrow invagination at cycle 13. These embryos had also been previously injected with Rhodamine-labeled monomeric actin, and time was provided for the monomeric actin to fully incorporate into furrows. At 1 min 20 s after Latrunculin injection, the levels of exogenous actin and GFP-Moesin were clearly diminished (Fig. 1 B), indicating loss of F-actin from the furrow. Quantification of the signal intensities at furrows areas indicated that 4 min after injection, the Rhodamine-actin and GFP-Moesin signals were reduced by 74.4 ± 6.6% (*n* = 3 embryos) and 78.8 ± 2.3% (*n* = 3 embryos), respectively (Fig. 1 C, furrow intensity calculation). In contrast, the fluorescence signals 4 min after injection in DMSO-injected

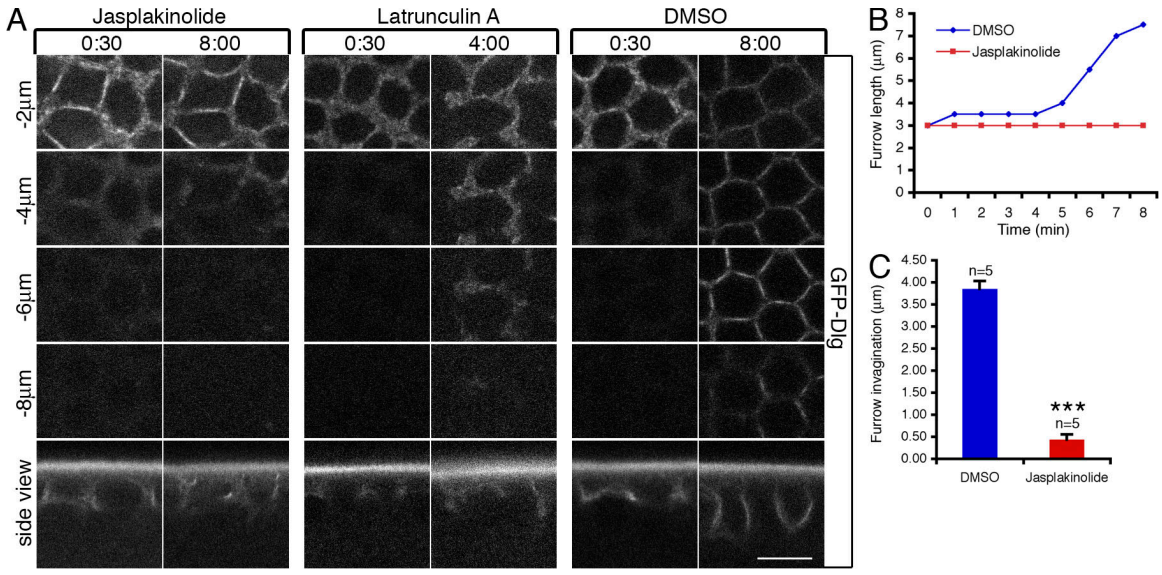

Figure 2. **F-actin turnover is required for furrow invagination.** (A) 1 mM Jasp, 2 mM LatA, or DMSO control were injected into GFP-Dlg embryos at cycle-13 early prophase (when furrow is ~3 µm in length), and furrow invagination was followed over time at depths from −2 µm to −8 µm below the embryo surface. (B) The lengths of invaginating furrows (y axis) over time (x axis) after 1 mM Jasp or DMSO injections in A. (C) Quantification of results in A. Increases in furrow lengths (in micrometers) 8 min after Jasp (n = 5 embryos) or DMSO (n = 5 embryos) injections were analyzed. ***, $P < 0.001$. Error bars represent SEM. Bar, 10 µm.

controls were reduced only by 0.9 ± 0.4% (Rhodamine-actin; $n = 3$ embryos) and 0.8 ± 0.3% (GFP-Moesin; $n = 3$ embryos).

To better understand actin dynamics at the furrow, we quantified turnover rates of F-actin at metaphase furrows using FRAP. Previous FRAP analyses on cleavage furrows could not differentiate the actin turnover rates at the preexisting furrow and at the ingressing furrow tips (Pelham and Chang, 2002; Guha et al., 2005; Murthy and Wadsworth, 2005). Our system enables viewing of preexisting furrows and furrow tips separately at defined z depths below the embryo surface, allowing examination of actin turnover exclusively in preexisting furrows and furrow tips, respectively. Monomeric Rhodamine-actin was injected into GFP-Moesin–expressing embryos and allowed to fully incorporate into existing furrows, and then these labels were photobleached. This experiment revealed that F-actin turnover is rapid in preexisting furrows, with a fluorescence recovery $t_{1/2}$ of 25.9 ± 1.8 s ($n = 10$ embryos) for GFP-Moesin and 17.9 ± 1.3 s ($n = 10$ embryos) for Rhodamine-actin (Fig. 1, D and E; and Video 1, available at http://www.jcb.org/cgi/content/full/jcb.200712036/DC1). Furthermore, the respective fluorescence labels returned to 83.8 ± 2.9% ($n = 10$ embryos) and 86.3 ± 3.5% ($n = 10$ embryos) of their prebleached intensities 80 s after photobleaching, indicating that most of the F-actin in the furrow turned over within that time period. Similar fluorescence recovery results were obtained when furrow tips were photobleached, with a $t_{1/2}$ of 24.2 ± 2.3 s ($n = 11$ embryos) for GFP-Moesin and 21.6 ± 1.6 s ($n = 11$ embryos) for Rhodamine-actin. Accordingly, 88.7 ± 5.7% ($n = 11$ embryos) of the GFP-Moesin and 92.3 ± 5.3% ($n = 11$ embryos) of the Rhodamine-actin intensities were recovered at the furrow tips 80 s after photobleaching. Collectively, with our experiments demonstrating actin polymerization and depolymerization activities at the metaphase furrows, these results indicate that metaphase and conventional cytokinesis furrows share the property of rapid F-actin turnover.

F-actin turnover is required for furrow invagination

To investigate the functional impact of actin turnover on furrow dynamics, we inhibited actin turnover by injecting Jasp (Jasplakinolide) or LatA into living embryos. The efficacy of Jasp was demonstrated by excess F-actin accumulation at the invaginating furrows when it was injected during cycle 13 in wild-type (WT) embryos expressing a GFP-Dlg (Discs-Large) transgene (Fig. S2, available at http://www.jcb.org/cgi/content/full/jcb.200712036/DC1; Quinones-Coello et al., 2007). Dlg has previously been used as a marker for cellularization membrane in *D. melanogaster* (Lee et al., 2003; Grosshans et al., 2005). Both furrow invagination, determined by the length of the furrow, and furrow integrity, indicated by the furrow ring structure behind the invaginating leading edge, were analyzed using this marker. Although furrow integrity was not perturbed, furrow invagination was blocked after Jasp injection (Fig. 2, A–C). In contrast, LatA injection permitted furrow invagination but caused gaps in the furrow ring structure (Fig. 2 A), which is reminiscent of a previous study demonstrating that the free ends of incomplete metaphase furrows in *nuf* mutant embryos extend normally (Rothwell et al., 1999). These reults indicate that depolymerization or destabilization of F-actin at the furrow is required for furrow invagination, whereas actin polymerization is required for maintaining furrow integrity.

F-actin is required for maintaining membrane integrity during furrow invagination

To further investigate the relationship between F-actin stability and membrane integrity, we injected LatA into embryos that were previously injected with Rhodamine-labeled actin and also expressed GFP-Dlg. As shown in Fig. 3 A, GFP-Dlg–marked

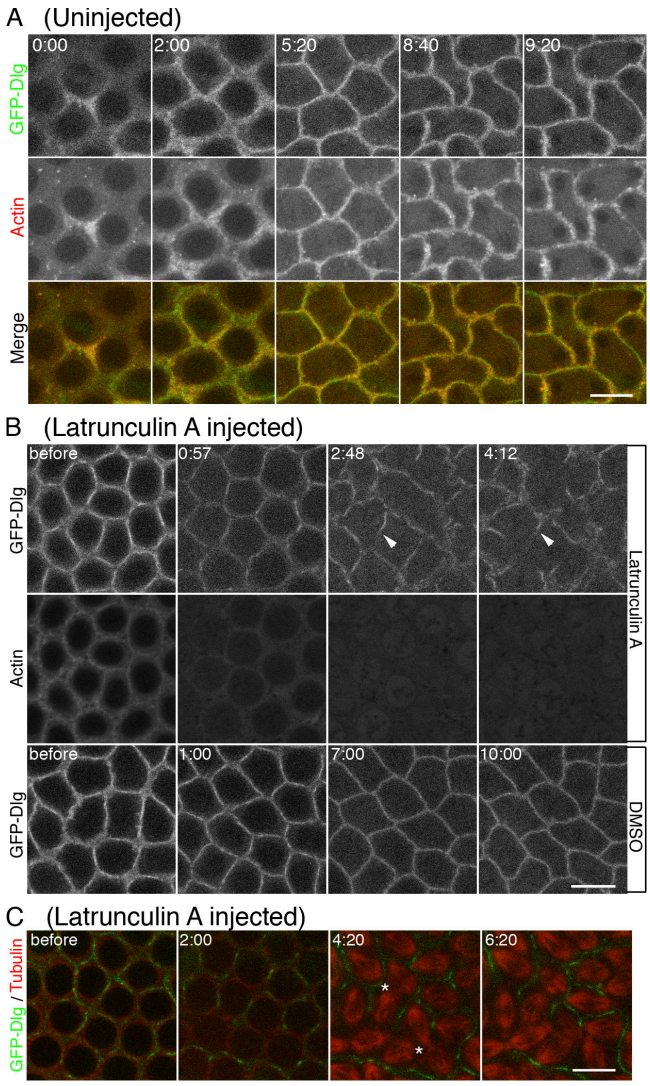

Figure 3. **F-actin is required for maintaining membrane integrity during furrow invagination.** (A) In untreated cycle-12 embryos, membrane (GFP-Dlg, green) is closely surrounded by F-actin (red) at the furrow. (B) 2 mM LatA or DMSO was injected at cycle-13 early prophase. GFP-Dlg–marked plasma membrane was progressively lost (arrowheads) as furrows invaginated in LatA-injected embryos (top row). Membrane loss started after most of the F-actin was lost at the furrow (middle row). (C) Furrow integrity was monitored relative to spindle spacing and dynamics (tubulin, red). Spindle fusion (asterisks) occurred where membrane (Dlg, green) was lost at the furrow. See Video 2 (available at http://www.jcb.org/cgi/content/full/jcb.200712036/DC1). Bars, 10 µm.

plasma membrane was closely surrounded by F-actin at the furrow in untreated WT embryos. LatA injection caused an immediate loss of F-actin signal intensity at the furrow (Fig. 3 B). Initially, the injection had no apparent effect on GFP-Dlg distribution, but by 3 min after injection, large gaps of GFP-Dlg–labeled membrane were visible (Fig. 3 B, arrowheads). These gaps became more extensive as furrow progression proceeded. The same effect on furrow membrane integrity was seen in older cellularizing embryos after disrupting F-actin at the furrow by LatA injection (Fig. S3 A, available at http://www.jcb.org/cgi/content/full/jcb.200712036/DC1). These studies indicate that in both cycle 13 and cellularization-stage embryos, F-actin loss at the furrow was followed by the loss of membrane integrity. To further verify these results, we analyzed the effect of LatA with a different plasma membrane marker, Spider-GFP, a casein kinase I which is associated with the plasma membrane (Frescas et al., 2006). As with the GFP-Dlg, LatA injection led to breaks in the previously contiguous Spider-GFP signal (Fig. S3 B). These data demonstrate that F-actin is required for maintaining membrane integrity at the invaginating furrow.

To examine the functional consequences of disrupted plasma membrane integrity after loss of F-actin, we injected LatA into living embryos carrying Rhodamine-labeled tubulin and GFP-Dlg to monitor the mitotic spindles and furrow membrane. As expected, LatA injection led to the formation of large gaps in the furrow membrane within 4 min after injection (Fig. 3 C and Video 2, available at http://www.jcb.org/cgi/content/full/jcb.200712036/DC1). Interestingly, mitotic spindles adjacent to those membrane gaps began fusing 4 min after LatA injection (Fig. 3 C, asterisks; and Video 2). However, mitotic spindles adjacent to partial or intact furrow membranes remained independent of one another (Fig. 3 C and Video 2). As most of F-actin was no longer associated with the remaining furrow membrane 4 min after LatA injection (Figs. 3 B and 1 B), these data indicate that plasma membrane, not F-actin, serves as the primary barrier separating neighboring spindles from one another.

Nuf is required to maintain furrow integrity

Previous studies have shown that the RE component Nuf is required for actin and membrane recruitment to the invaginating furrow (Rothwell et al., 1998; Riggs et al., 2003). To address why *nuf* mutant embryos exhibit actin as well as membrane defects, we examined furrow formation in living nuf^{1} (the strongest *nuf* allele; see Materials and methods) embryos expressing GFP-Moesin. In WT control embryos expressing GFP-Moesin, no breaks were seen at furrows during furrow invagination (Fig. 4 A). In contrast, it appears that the F-actin loss initially occurs basally and progresses apically at the furrows in *nuf* embryos (Fig. 4 B, arrowheads). Additionally, F-actin loss expands laterally (Fig. 4 B, arrows; and Video 3, available at http://www.jcb.org/cgi/content/full/jcb.200712036/DC1). At metaphase, when furrows have invaginated to their maximal length, breaks were seen throughout the entire length of the furrow resulting in spindle fusions (Fig. 4 B, asterisks; and Video 3). Loss of F-actin stability was also seen in *Rab11* embryos during metaphase furrow invagination (Fig. 4 C) and in *nuf* embryos during cellularization (Fig. S4 A, available at http://www.jcb.org/cgi/content/full/jcb.200712036/DC1). Given that Rab11 is required for RE integrity, these results together indicated that the RE is required to maintain F-actin stability at the invaginating furrows.

Previous work has shown membrane breaks at the furrows in *nuf* and *Rab11* mutant embryos (Rothwell et al., 1998; Riggs et al., 2003). Our live analysis of membrane dynamics using GFP-Dlg in *nuf* embryos showed a loss of membrane over time (Fig. 4 D, arrowheads). This indicates that, similar to F-actin, furrow membrane is not stably maintained. To investigate if membrane integrity is dependent on F-actin stability, we injected *nuf* embryos expressing GFP-Dlg with Rhodamine-actin. This live analysis indicated

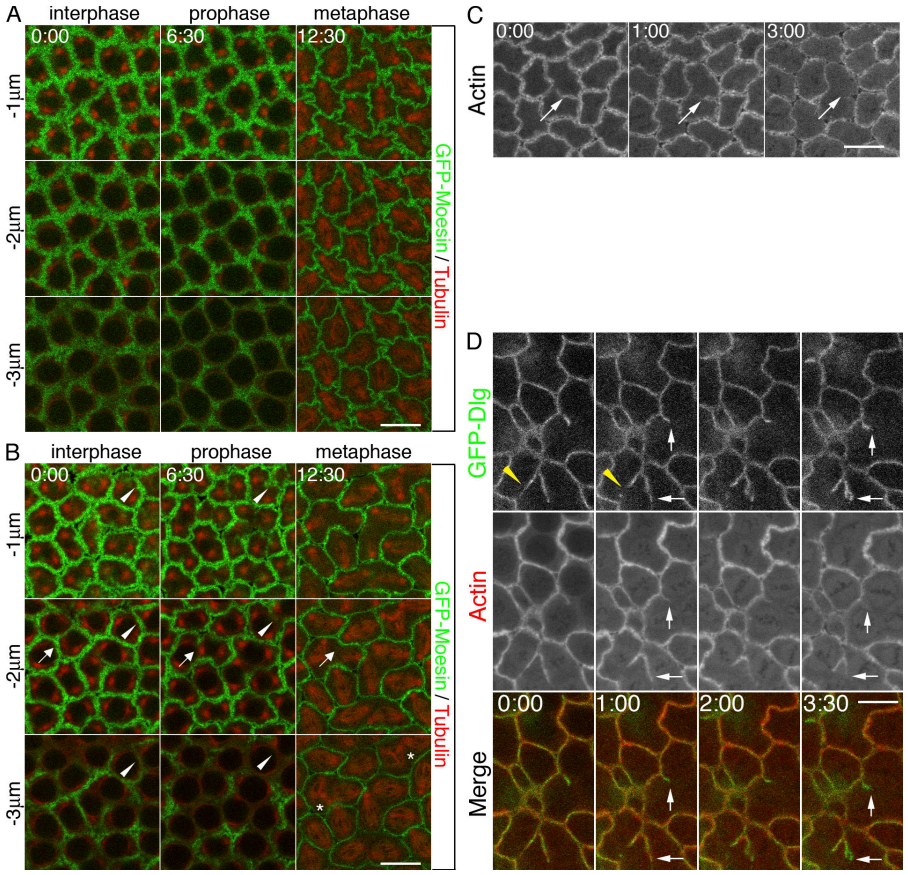

Figure 4. **The RE is required for furrow maintenance.** (A) GFP-Moesin (green) and Rhodamine-tubulin (red) in WT embryos. From cycle-13 interphase to metaphase, three z sections are shown from 1 to 3 µm below the cortex. (B) Same experiment as in A in *nuf* embryos. F-actin was progressively lost at the furrow (arrows) as furrows invaginated, and this loss started at the sections closer to the invaginating tips (arrowheads; compare 6:30 to 0:00 at different depths). Spindle fusions (asterisks) occurred where furrows were broken. See Video 3 (available at http://www.jcb.org/cgi/content/full/jcb.200712036/DC1). (C) Time-lapse images of *Rab11* cycle-13 furrow progression. Rhodamine-labeled actin was gradually lost at the furrow (arrows). (D) GFP-Dlg (green) and Rhodamine-actin (red) in *nuf* embryos. Yellow arrowheads indicate loss of membrane at the furrow over time. Loss of F-actin at the furrow generally precedes loss of membrane (arrows). See Video 4 (available at http://www.jcb.org/cgi/content/full/jcb.200712036/DC1). Bars, 10 µm.

that F-actin loss at the furrow generally precedes membrane loss (Fig. 4 D, arrows; and Video 4, available at http://www.jcb.org/cgi/content/full/jcb.200712036/DC1). In contrast, membrane loss never precedes F-actin loss in *nuf* embryos. This is in accord with our observation that LatA-induced loss of F-actin precedes loss of membrane at the furrow and suggests that F-actin loss in *nuf* embryos may be the cause of membrane loss at the furrow.

Genetically reducing actin depolymerization rescues the furrow defects observed in *nuf* embryos

The striking reduction of furrow F-actin in *nuf* mutant embryos raises the question: does Nuf promote actin polymerization or stabilization at the furrow? If Nuf has such a function, one prediction would be that reducing actin depolymerization should suppress furrow defects in *nuf* embryos. Cofilin is a well-known actin depolymerizer in a variety of processes that require remodeling of the actin cytoskeleton including cell migration and cytokinesis (Ono, 2007). Homozygous mutations for *tsr* (*twinstar*), the *D. melanogaster* Cofilin homologue, are zygotic lethal and cause cytokinesis defects in contractile ring disassembly (Gunsalus et al., 1995). To test whether *tsr* can rescue the *nuf* phenotype, we collected eggs laid by female flies homozygous for *nuf* and heterozygous for *tsr* and then examined them for furrow and spindle morphology during cycle 13 in early embryogenesis. When *twinstar*-null alleles tsr^{N96A} and tsr^{N121} (Ng and Luo, 2004) were crossed into the homozygous nuf^{1} background (e.g., $tsr^{N96A}/Cy;\ nuf^{1}/nuf^{1}$), all the female ovaries had strong membrane defects in the egg chambers that prevented them from undergoing embryonic development (unpublished data). When the hypomorphic tsr^{1} allele (Gunsalus et al., 1995) was introduced into the nuf^{1} background, the ovaries exhibited milder membrane defects, and a portion of eggs was able to develop after fertilization: 21% (n = 1,551 eggs) of the total eggs laid by $tsr^{1}/Cy;\ nuf^{1}/nuf^{1}$ females hatched and of these larvae, 75% (n = 331 larvae) developed into adult flies, compared with a 0% (n = 547 eggs) hatch rate of eggs laid by nuf^{1} females. Moreover, these $tsr^{1}/Cy;\ nuf^{1}/nuf^{1}$ embryos displayed much less severe defects than nuf^{1} embryos, with fewer furrow breaks and spindle fusions in metaphase and cellularizing furrows (Fig. 5, A and B; Video 5, available at http://www.jcb.org/cgi/content/full/jcb.200712036/DC1; and not depicted). The suppression of *nuf* phenotype by reducing Twinstar dosage supports a role for Nuf in promoting actin polymerization at the furrow.

Drug-induced actin polymerization and stabilization suppresses the furrow defects exhibited by *nuf* embryos

To further test the possibility that Nuf promotes furrow integrity by promoting actin polymerization, we artificially enhanced actin nucleation and polymerization by injecting Jasp into *nuf* embryos and monitored furrow membrane dynamics with GFP-Dlg. In contrast to *nuf* control embryos (Fig. 5 C, top row; and Video 6, available at http://www.jcb.org/cgi/content/full/jcb.200712036/DC1), *nuf* embryos injected with Jasp during nuclear cycle-13 early prophase (when furrow integrity is

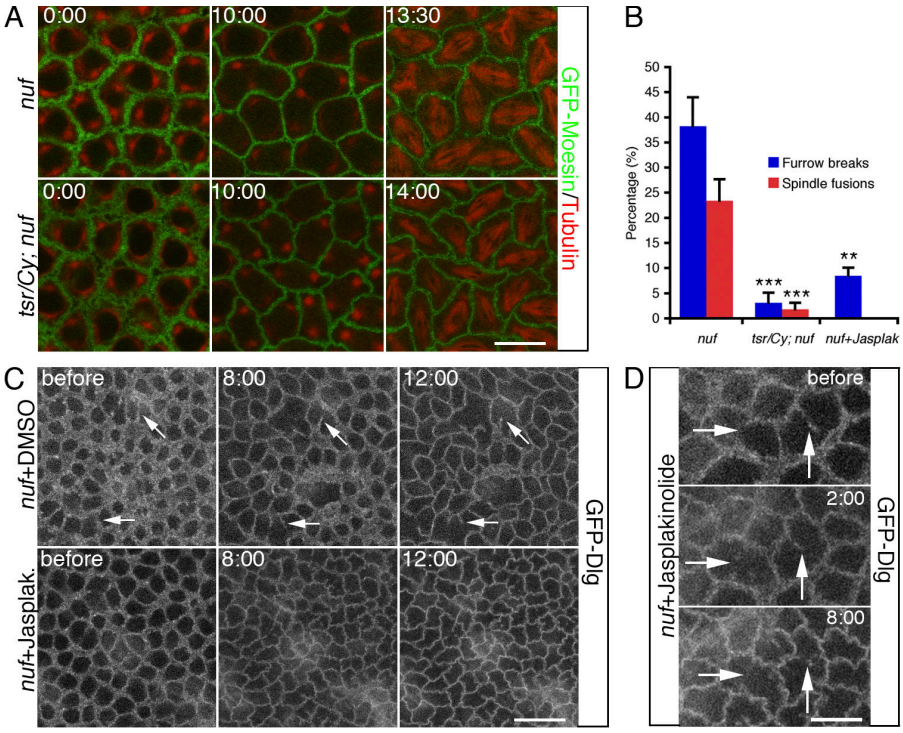

Figure 5. **Reducing actin depolymerization by *tsr* or promoting actin polymerization by Jasp ameliorates the furrow defects observed in *nuf* embryos.** (A) Green, GFP-Moesin; Red, tubulin. Compared with nuf^{1} embryos (top row, the same embryo as shown in Fig. 4 A), $tsr^{1}/Cy; nuf^{1}$ embryos (bottom row) exhibited normal furrow structures from interphase to metaphase during cycle 13. For full movie, see Video 5 (available at http://www.jcb.org/cgi/content/full/jcb.200712036/DC1). (B) Quantifications of results in A and C. At metaphase cycle 13, furrow break index and spindle fusion index in nuf^{1} (N = 12 and *n* = 1,378), $tsr^{1}/Cy; nuf^{1}$ (N = 8 and *n* = 1,010), and nuf^{1} + Jasp (N = 7 and *n* = 846) embryos. N, total embryos examined; n, total nuclei/mitotic spindles analyzed. **, $P < 0.01$; ***, $P < 0.001$. Error bars represent SEM. (C and D) nuf^{1} embryos expressing GFP-Dlg were injected with either 1 mM Jasp or DMSO at cycle-13 early prophase. (C) Jasp-injected *nuf* embryos show very few furrow breaks at metaphase, whereas DMSO-injected *nuf* embryos display extensive discontinuous furrows resulting from progressive loss of furrow membrane (arrows). See Videos 6 and 7 (available at http://www.jcb.org/cgi/content/full/jcb.200712036/DC1). (D) The membrane loss before Jasp injection in nuf^{1} embryos was not compensated after Jasp treatment (arrows). Bars: (A and D) 10 µm; (C) 20 µm.

still relatively normal) showed almost no further loss of membrane (Fig. 5, B and C [bottom row]; and Video 7) or F-actin (Fig. S4 B) at the metaphase furrows. In regions where furrow membrane was already lost before injection, Jasp did not induce new membrane growth to fill the furrow gaps (Fig. 5 D), which is consistent with our finding that Jasp functions to stabilize actin cytoskeleton and its associated plasma membrane (Fig. 2, A–C). Jasp also disrupted spindle formation (Fig. S4 B), and thus spindle fusion was not pursued in these Jasp-treated *nuf* embryos. In conclusion, actin assembly and stabilization driven by Jasp suppresses the *nuf* phenotype, further supporting a role for Nuf in promoting actin polymerization at the furrow, which in turn stabilizes furrow membrane.

Up-regulating RhoA activities compensates the furrow defects observed in *nuf* embryos

Insight into the mechanism by which Nuf promotes actin polymerization comes from the observation that overexpression of Nuf suppresses the reduced Rho signaling in the eye (Gregory et al., 2007). In addition, both RhoA and Nuf are crucial in actin remodeling at the furrows (Crawford et al., 1998; Prokopenko et al., 1999; Riggs et al., 2003; Padash Barmchi et al., 2005; Piekny et al., 2005). We examined if RhoA and Nuf share a common function in promoting furrow maintenance by testing if reduced RhoA activity produces the *nuf* phenotype. The Rho inhibitor C3 exotransferase was injected into cycle-13 prophase embryos expressing GFP-Dlg. C3 transferase has been widely used to block Rho signaling in different systems including cellularization and conventional cytokinesis (Crawford et al., 1998; Bement et al., 2005). Similar to embryos deficient for Nuf or injected with LatA, C3-treated embryos induced membrane loss over time, which eventually led to neighboring spindle fusions (Fig. 6 A and Video 8, available at http://www.jcb.org/cgi/content/full/jcb.200712036/DC1). Importantly, loss of F-actin also precedes loss of membrane at the furrows after C3 injection (Fig. 6 B). This indicates that, similar to *nuf* embryos, blocking Rho activity induces loss of F-actin stability at the furrow, which results in loss of membrane integrity. The phenotypes of reducing Rho or Nuf function are strikingly similar, suggesting that Nuf functions within a Rho pathway to promote furrow integrity.

To test if RhoA and Nuf function in the same pathway for furrow maintenance, a constitutively active mammalian RhoA(Q63L) protein was injected into *nuf* embryos. *D. melanogaster* RhoA is highly related to its mammalian counterpart (Hariharan et al., 1995) and studies have shown that mammalian RhoA constructs are effective tools to inhibit the *D. melanogaster* RhoA pathway. Injection or expression of the constitutively active or dominant-negative mammalian RhoA in the *D. melanogaster* embryo specifically disrupts endogenous RhoA signaling (Crawford et al., 1998; Harden et al., 1999). RhoA(Q63L) injection into *nuf* embryos suppressed the *nuf* phenotype near the site of injection, where furrows were formed and maintained normally (Fig. 6 C, arrow; and Video 9, available at http://www.jcb.org/cgi/content/full/jcb.200712036/DC1). In regions distant from the injection site, typical *nuf*-induced furrow defects were observed (Fig. 6 C, arrowheads; and Video 9). To verify the localized RhoA-GTP rescue, we performed injections in different embryonic regions. Rescue always correlated with site of injection during both cycle 13 (*n* = 6, 5, and 6 embryos for anterior, posterior, and central injection, respectively) and cellularization

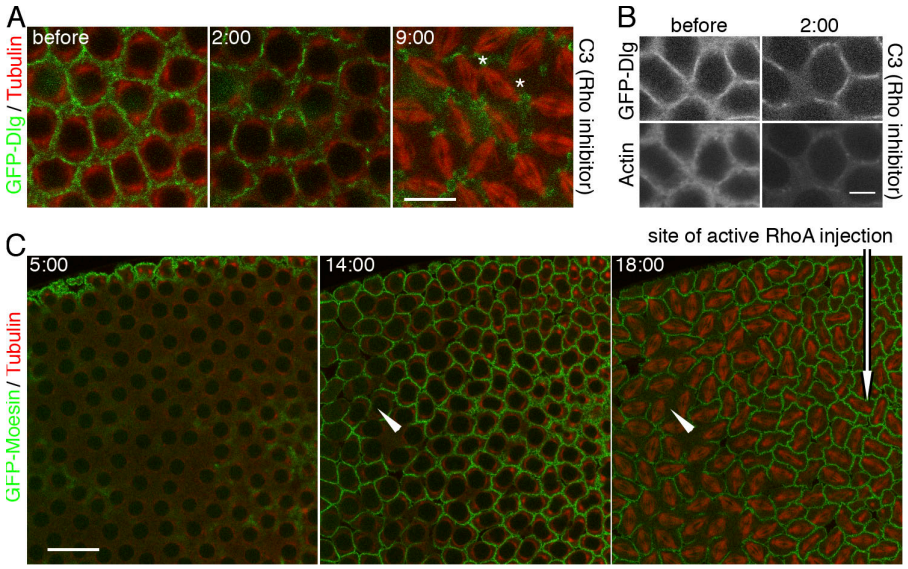

Figure 6. **Nuf functions within the RhoA pathway to promote furrow integrity.** (A and B) 1 mg/ml C3 transferase was injected at cycle-13 early prophase. (A) GFP-Dlg–marked furrow membrane (green) was progressively lost and eventually led to spindle fusions (red, asterisks). See Video 8 (available at http://www.jcb.org/cgi/content/full/jcb.200712036/DC1). (B) 2 min after C3 injection, most of the F-actin has been lost from the furrow (bottom). In contrast, membrane loss has just started (top). (C) 1 mg/ml RhoA(Q63L) was injected into *nuf* embryos at cycle-13 early interphase. Green, GFP-Moesin; red, tubulin. At metaphase (18:00), normal furrow structures were maintained in the region close to injection site (arrow); however, loss of F-actin at the furrows is evident further away from the site of injection (arrowheads). See Video 9 (available at http://www.jcb.org/cgi/content/full/jcb.200712036/DC1). Bars: (A) 10 μm; (B) 5 μm; (C) 20 μm.

(Fig. S4 C). These data suggest Nuf acts upstream of RhoA-mediated actin polymerization at the furrow.

Nuf is required for proper recruitment and localization of RhoGEF2, an actin remodeler, to the furrow

A plausible mechanism by which Nuf functions within the RhoA pathway is by regulating recruitment of the *D. melanogaster* maternal RhoGEF, known as RhoGEF2. Fly embryos mutant for RhoGEF2, a Rho1 activator, produced defects in actin organization at the furrow similar to those in *nuf* embryos (Fig. 7 A; Grosshans et al., 2005; Padash Barmchi et al., 2005). In addition, because RhoGEF2 localizes to the furrow as cortical puncta (Fig. 7 B; Padash Barmchi et al., 2005), it is possible that Nuf-mediated endosomal vesicle trafficking is responsible for recruiting RhoGEF2 to the furrows.

To test this, RhoGEF2 localization was examined in WT and *nuf* mutant embryos that were also labeled with Dlg to mark the furrow membrane. In WT embryos, RhoGEF2 is concentrated at the furrow and in punctate structures around the furrow (Fig. 7 B). Line plot quantifications of signal intensities crossing the furrows showed that both RhoGEF2 and Dlg have a single peak of signal intensity at the furrow (Fig. 7 C). However, in *nuf* embryos, RhoGEF2 localization is abnormally diffuse around the furrow (Fig. 7 B) and RhoGEF2 is no longer distributed as a single focused intensity peak (Fig. 7 C). In addition, RhoGEF2 signal intensity does not generally correlate to the Dlg peak in *nuf* embryos (Fig. 7 C). Similar diffuse RhoGEF2 localization was evident in *Rab11* mutant embryos (Fig. 7, B and C), suggesting that recruitment and localization of RhoGEF2 is mediated by Nuf and Rab11 through the RE.

RhoGEF2 mislocalization could be a direct consequence of removing Nuf activity or an indirect consequence of gross furrow abnormalities. We therefore examined the localization of other furrow components in *nuf* mutant embryos. Unlike RhoGEF2, the core furrow components within the RhoA pathway, Rho1 and Diaphanous, generally concentrated in furrow regions where F-actin was properly localized (Fig. 7, D and E and Fig. S5, available at http://www.jcb.org/cgi/content/full/jcb.200712036/DC1). Furthermore, we tested the localization of RhoGEF2 together with another core furrow component, Anillin, in *nuf* embryos. Anillin is a multidomain protein that is essential for cytokinesis and plays an important role in scaffolding furrow components (Field et al., 2005). It localizes to the metaphase furrow preceding F-actin (Field and Alberts, 1995) and in *nuf* embryos, it localizes to regions of the furrows lacking F-actin during early furrow formation (Fig. 7 F, arrows; Rothwell et al., 1998). Therefore, Anillin is a good marker to indicate furrow integrity. Our staining showed that during early furrow formation, RhoGEF2 was diffusely localized at the furrow in regions where Anillin was properly localized (Fig. 7 F, arrows). Because RhoGEF2 was mislocalized in regions that show aspects of normal furrow structure, the data indicate that RhoGEF2 mislocalization in *nuf* embryos is caused by a lack of Nuf activity. Among the other furrow components tested in this and previous studies (Rothwell et al., 1998), there is a correlation between the mislocalization of furrow components and F-actin defects. Therefore, RhoGEF2 is unique in this respect because RhoGEF2 mislocalization is not limited to furrow regions with F-actin defects.

Nuf interacts genetically with RhoGEF2 and its downstream actin remodelers

Functional test for interaction between Nuf and the RhoA pathway were performed through dosage-sensitive genetic interactions between null alleles of *nuf* and several genes involved in actin remodeling (Fig. 7 G and Table I). Female flies singly heterozygous for *nuf* or any of these actin-remodeling mutations gave rise to embryos with minor furrow defects (Table I). However, double heterozygotes for nuf^{1} and a mutation in any of the four components of the RhoGEF2–Rho1 pathway yielded severe furrow defects (Fig. 7 G and Table I). For example, *RhoGEF2/+; nuf/+* embryos displayed very weak furrows distal to the centrosomes, whereas *Rho1/+; nuf/+* embryos exhibited extensive furrow breaks (Fig. 7 G, arrows). Likewise, *RhoGEF2/Rho1* embryos also displayed

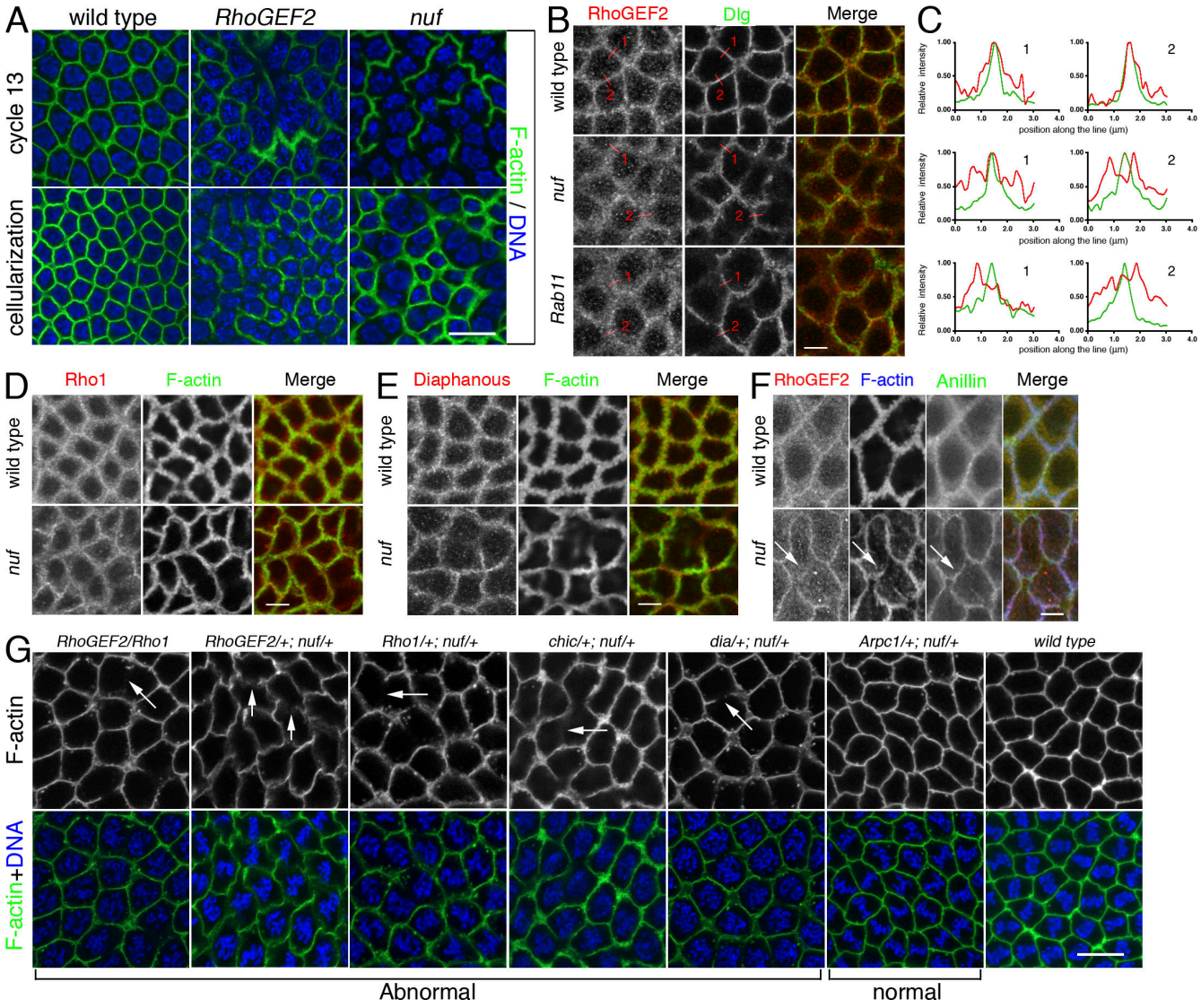

Figure 7. **Nuf is required for proper RhoGEF2 recruitment to the furrow.** (A) Images of fixed WT, *RhoGEF2*, and *nuf* embryos are shown in cycle-13 metaphase and cellularization (staged by DNA, blue) at the sections crossing the furrow. (B) Compared with WT, RhoGEF2 is more diffuse at the furrow in *nuf* and *Rab11* embryos at cycle-13 prophase. Green, F-actin; red, RhoGEF2. (C) Line plots of RhoGEF2 (red curves) and Dlg (green curves) signal intensities (normalized to the maximum signal of each plot into a 0–1 scale) crossing the furrows (red lines in B). WT exhibited a single focused RhoGEF2 peak corresponding to the Dlg peak. In *nuf* and *Rab11* embryos, RhoGEF2 showed unfocused peaks that did not generally correspond with the Dlg peak. (D and E) Rho1 and Diaphanous (red) are not concentrated in furrow regions lacking F-actin (green) but localize properly at regions maintaining F-actin in *nuf* embryos. (F) At cycle-13 interphase, RhoGEF2 (red) is diffusely localized around the furrow, whereas Anillin (green) is localized normally (arrows). (G) Nuf shows dominant genetic interactions with components of the RhoGEF2–Rho1 pathway. Cycle-13 prometaphase or metaphase embryos (staged by DNA; blue) derived from females with different genetic background were stained with phalloidin to show the furrow structure. (*RhoGEF2/Rho1*), (*RhoGEF2/+; nuf/+*), (*Rho1/+; nuf/+*), (*chic/+; nuf/+*), and (*dia/+; nuf/+*) embryos display abnormal furrow morphologies (arrows indicate furrow breaks or weak furrows), whereas (*Arpc1/+; nuf/+*) embryos have relatively normal furrow morphology. Summary of phenotypic frequencies is shown in Table I. Bars: (A and G) 10 μm; (B–F) 5 μm.

breaks, reflecting defects in furrow maintenance. Nuf also showed strong genetic interactions with Chickadee, the fly Profilin homologue, and Diaphanous, the fly homologue of Formin (Fig. 7 G and Table I). Both Profilin and Formin have been shown to act downstream of RhoA during cytokinetic furrow formation (Castrillon and Wasserman, 1994; Chang et al., 1997; Giansanti et al., 1998; Afshar et al., 2000). These results indicate that that Nuf regulates furrow stability through the Rho1 pathway. The genetic interactions appear to be specific because other maternal effect mutations, such as *grp*, *rok*, and *cdc2* (unpublished data), showed no prominent furrow defects in combination with *nuf*. The Arp2/3 complex has also been shown to drive actin polymerization for metaphase furrow assembly (Stevenson et al., 2002). Genetic interactions were tested between *Arpc1* (Hudson and Cooley, 2002), which encodes the p40 subunit of Arp2/3, and *nuf*; however, no obvious furrow defects were observed (Fig. 7 G and Table I). Among several possible interpretations, the strong dominant genetic interactions between Nuf, RhoGEF2, and Rho1 support a model in which these proteins cooperate in a common pathway to promote actin polymerization and furrow maintenance.

Table I. **Summary of furrow phenotypic frequencies in Fig. 7 G**

Maternal genotypes	Weak furrow	Very weak furrow	With breaks in furrow	Normal furrow morphology	Total embryos examined
WT	0	0	0	35 (100%)	35
nuf^{1}/+	3 (11%)	1 (4%)	0	23 (85%)	26
RhoGEF2$^{4.1}$/+	3 (25%)	0	0	9 (75%)	12
Rho1^{72O}/+	1 (13%)	0	0	7 (87%)	8
chic^{221}/+	0	0	0	12 (100%)	12
dia^{5}/+	1 (8%)	0	0	12 (92%)	13
Arpc1^{Q25sd}/+	0	0	0	12 (100%)	12
RhoGEF2$^{4.1}$/*Rho1*^{72O}	3 (23%)	3 (23%)	7 (54%)	0	13
RhoGEF2$^{4.1}$/+; *nuf*^{1}/+	7 (39%)	7 (39%)	0	4 (22%)	18
Rho1^{72O}/+; *nuf*^{1}/+	3 (25%)	1 (8%)	5 (42%)	3 (25%)	12
chic^{221}/+; *nuf*^{1}/+	4 (31%)	2 (15%)	3 (23%)	4 (31%)	13
dia^{5}/+; *nuf*^{1}/+	3 (30%)	0	5 (50%)	2 (20%)	10
Arpc1^{Q25sd}/+; *nuf*^{1}/+	2 (18%)	0	0	9 (82%)	11

The number of embryos exhibiting the phenotype under each group is shown and the frequency is also indicated.

Discussion

F-actin rapidly turns over during myosin II–independent furrow invagination

Although the composition and dynamics of the cortical cytoskeleton associated with metaphase and cellularization furrows invagination have been well characterized (Foe et al., 1993, 2000), much remains unknown about the mechanisms driving actin dynamics and distribution at these furrows. To address this issue, we determined the turnover rates of F-actin by performing FRAP analysis on the furrow-associated F-actin located at the tip and 1–2 μm behind the leading edge of the furrow. These studies demonstrate that GFP-Moesin, an F-actin binding protein, and injected Rhodamine-labeled actin are rapidly turned over. The turnover rates are comparable with turnover rates observed in LLCPK1 epithelial cell contractile ring (26 s; Murthy and Wadsworth, 2005), normal rat kidney cell equatorial cortex (12–15 s; Guha et al., 2005) and fission yeast contractile ring (~25 s; Pelham and Chang, 2002). Furthermore, rapid incorporation of G-actin into preexisting furrow-actin filaments and rapid disappearance of F-actin from preexisting furrows after LatA treatment indicate that both actin polymerization and depolymerization contribute to F-actin turnover at the furrow. These studies are in accord with previous work demonstrating rapid turnover of actin at the cleavage furrows (Pelham and Chang, 2002; Guha et al., 2005; Murthy and Wadsworth, 2005). Although previous work focused on F-actin turnover specifically at the contractile ring, our studies demonstrate that F-actin also turns over in a myosin-free zone well behind the leading edge of the ingressing furrow (Royou et al., 2004).

Actin turnover coordinates furrow invagination with furrow integrity

Although it is likely that rapid actin turnover will prove to be a conserved feature of cytokinetic furrows, its functional significance remains unclear. F-actin turnover may be required for proper actomyosin-based constriction of the contractile ring, as this structure decreases in volume as constriction proceeds (Schroeder, 1972). However, the F-actin turnover observed behind the leading edge of *D. melanogaster* metaphase and cellularization furrows is likely to have additional function, as furrow ingression is not dependent on actomyosin-based contraction (Royou et al., 2004). Rather, ingression of these furrows relies largely on vesicle-mediated membrane addition (Lecuit and Wieschaus, 2000; Sisson et al., 2000; Pelissier et al., 2003; Riggs et al., 2003). Consequently, we analyzed the relationship between F-actin turnover, furrow membrane stability, and ingression by simultaneously monitoring plasma membrane and F-actin dynamics. We find that LatA injection results in an immediate loss of F-actin. In addition, the loss of F-actin after LatA treatment always precedes loss of furrow membrane integrity. These results indicate that cortical F-actin is critical for maintaining furrow membrane integrity. Previous studies demonstrated that LatA-induced disruption of F-actin results in relaxation of the cleavage furrow (Murthy and Wadsworth, 2005). Our studies suggest that this relaxation may be in part caused by loss of furrow membrane integrity. Our finding also provides a possible explanation for the observation that mutants in Anillin, an F-actin bundling protein, produce large gaps in the plasma membrane of the cellularization furrow (Field et al., 2005). These gaps may also be a direct consequence of F-actin loss.

To understand the functional significance of F-actin turnover at the furrow, we injected Jasp, a drug that stabilizes F-actin by inhibiting F-actin turnover (Bubb et al., 2000; Murthy and Wadsworth, 2005). Jasp resulted in a robust accumulation of F-actin at the furrows but did not disrupt furrow integrity. However, it prevented both furrow progression and regression, indicating an increase in furrow stability. This result is consistent with studies in other systems demonstrating that excess accumulation or stabilization of F-actin significantly slowed or blocked progression of the cleavage furrows (O'Connell et al., 2001; Murthy and Wadsworth, 2005; Mukhina et al., 2007). Those studies were performed in cells in which furrow advancement requires actomyosin-based contraction at the contractile ring and, thus, it remained unclear if the block of furrow

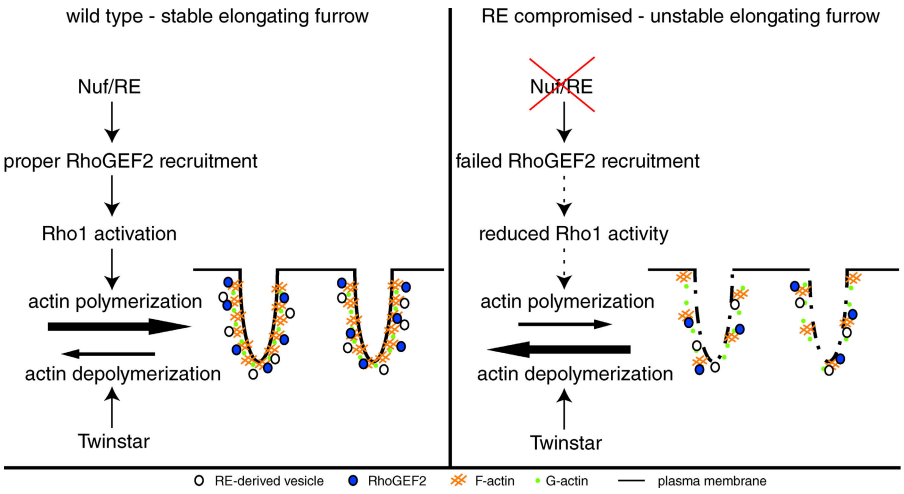

Figure 8. **Model.** In WT embryos, Nuf promotes actin polymerization at the invaginating furrow by properly localizing RhoGEF2 to the furrow, where it activates Rho1. Up-regulating actin polymerization stabilizes furrow membrane. In *nuf* mutant embryos, failed RhoGEF2 recruitment results in insufficient actin polymerization. This in turn results in loss of furrow membrane integrity.

progression was solely caused by inhibition of contractile ring constriction. Because furrow invagination in the early *D. melanogaster* embryo is primarily the result of vesicle-mediated membrane addition and it does not require actomyosin-based constriction, the Jasp-induced block of metaphase furrow progression is likely caused by inhibition of processes other than actomyosin-based constriction.

One explanation for these results comes from studies demonstrating that cortical F-actin acts as a barrier preventing vesicles from gaining access to docking and fusion sites at the plasma membrane. Studies suggest that transient depolymerization of F-actin at the membrane–actin cytoskeleton interface facilitates membrane addition to the furrow (Eitzen, 2003). The recent realization that vesicle-mediated membrane addition plays an important role in ingression of the cytokinetic furrow (Albertson et al., 2005) raises the possibility that F-actin turnover is required to facilitate vesicle-mediated membrane fusion. Our studies suggest that F-actin turnover at the cytokinetic furrow is required to facilitate vesicle-mediated membrane growth while simultaneously providing structural integrity to the newly invaginated membrane.

Nuf maintains furrow stability through promoting actin polymerization

Our studies of F-actin dynamics also provide insights into the role of Nuf, a Rab11 effector, during invagination of the metaphase and cellularization furrows. Nuf and its mammalian homologue FIP3 are required for the structural integrity of the RE (Riggs et al., 2003; Emery et al., 2005; Horgan et al., 2007). Disruption of Nuf/FIP3 function results in a failure to complete cytokinesis, and *rab11* mutants produce a similar phenotype (Riggs et al., 2003; Wilson et al., 2005). These results, along with cytological observations of vesicle distributions (Rothwell et al., 1999; Riggs et al., 2003; Wilson et al., 2005), indicate that vesicles derived from the RE are an important source of membrane during furrow formation. Although Rab11 remains associated with the RE throughout the cell cycle, Nuf exhibits a cell cycle–regulated Dynein-dependent recruitment to the RE (Riggs et al., 2007). Nuf is associated with the RE only at those phases of the cell cycle in which the furrows are invaginating. It is possible that the cell cycle–regulated association of Nuf with Rab11 may stimulate vesicle delivery to the invaginating furrows.

A puzzling feature of the *nuf* and *Rab11* mutant phenotypes is that they cause severe defects in furrow F-actin organization as well as defects in membrane integrity (Riggs et al., 2003). The LatA injection studies described in the previous section raise the possibility that the defects in F-actin organization precede and cause the membrane defects observed in *nuf* and *Rab11* mutant embryos. Support for this idea comes from our finding that the initial defect in *nuf* embryos is the formation of large gaps in the invaginating furrow-associated F-actin. Shortly after loss of F-actin, we observed loss of membrane integrity in the same region. This phenotype is strikingly similar to that observed in LatA-treated embryos: an immediate loss of F-actin followed by a loss of membrane integrity. These results suggest that a primary function of Nuf during furrow invagination is to maintain high levels of F-actin along the length of the furrows. In addition, we conclude that at least some of the observed membrane defects in *nuf* embryos are a direct consequence of the defects in F-actin organization (Fig. 8).

Because F-actin is rapidly turning over, the abundance of F-actin in any given region of the furrow depends on the relative polymerization and depolymerization rates. Thus, one explanation for the failure to maintain F-actin at the furrows in *nuf* embryos is a disruption in the relative rates of polymerization and depolymerization. To test this idea, we artificially increased the rate of actin polymerization in *nuf* embryos by injecting Jasp. The Jasp injections prevented loss of furrow-associated F-actin in *nuf* embryos. Significantly, in addition to maintaining F-actin integrity, the Jasp injections also maintained furrow membrane integrity in *nuf* embryos. We confirmed this result by genetically reducing the dosage of Twinstar/Cofilin in *nuf* embryos. Cofilin is known to sever and depolymerize F-actin during cell migration and cytokinesis (Ono, 2007). Thus, reducing Cofilin dosage is likely to reduce the rate of actin depolymerization and increase cortical F-actin levels. In accord with this reasoning, we find that reducing the dosage of Twinstar, the *D. melanogaster* homologue of cofilin, dramatically suppresses both the F-actin and membrane defects observed in *nuf* embryos. In contrast to embryos carrying the

normal dosage of *twinstar*, *nuf* embryos with reduced dosage of *twinstar* exhibited relatively normal metaphase and cellularization furrows. Normally, none of the eggs hatch from *nuf* embryos. However, in *nuf* embryos with reduced levels of Twinstar, significant egg hatch was observed and a large proportion of these gave rise to adults. These findings strongly support the idea that the primary defect in *nuf* embryos is a failure to maintain sufficient levels of F-actin at the plasma membrane during furrow invagination. The loss of F-actin ultimately results in loss of integrity in the plasma membrane.

RE-derived vesicles deliver actin polymerization activity to the invaginating furrows

Our studies raise the issue of the mechanism by which Nuf promotes F-actin stability during furrow invagination. Previous studies demonstrated that vesicles near the invaginating furrow are often associated with F-actin, raising the possibility that F-actin and vesicles are delivered as a unit to the invaginating furrows (Rothwell et al., 1999). It may be that as F-actin is depolymerized at the furrow, new F-actin is directly supplied by vesicle-mediated delivery. Support for this idea comes from studies in cultured animal cells demonstrating that F-actin is transported along the cortex to the ingressing furrow (Cao and Wang, 1990). It may be that, like in the *D. melanogaster* embryo, this cortically transported F-actin is vesicle associated.

An alternative explanation is based on the idea that RE-derived vesicles destined for invaginating furrows may carry potent actin remodelers (Riggs et al., 2003). Support for this model is provided by several studies demonstrating that RhoGEF2 and its downstream effectors Rho1 and Diaphanous are required for proper actin remodeling at the metaphase and cellularization furrows (Crawford et al., 1998; Afshar et al., 2000; Grosshans et al., 2005; Padash Barmchi et al., 2005). Analysis of *RhoGEF2* mutants was particularly intriguing because the resulting gaps in the furrow-associated F-actin were strikingly similar to those observed in *nuf* and *Rab11* embryos. In addition, RhoGEF2 was observed not only at the invaginating membrane but also in puncta throughout the cortex, raising the possibility that it is delivered through vesicles (Padash Barmchi et al., 2005).

In this paper, we find that RhoGEF2 delivery and localization at the metaphase furrows require Nuf and Rab11. In *nuf* embryos, although Rho1 and Diaphanous were mislocalized only in the region where furrow was disrupted, RhoGEF2 was globally diffuse around the furrow, implying a specific role for the RE in delivering RhoGEF2. We also find that treating embryos with the Rho inhibitor C3 exotransferase produces phenotypes similar to *nuf*, in which loss of F-actin at the furrow precedes membrane loss. Conversely, injecting constitutively active RhoA into *nuf* embryos rescues the *nuf*-induced furrow defects specifically at the injection site.

Synthetic genetic interactions between Nuf and the RhoGEF2–Rho1 pathway further support the model that vesicles derived from RE ferry both membrane and actin-remodeling activity to the invaginating furrow. This model emphasizes an important role for the RE in linking membrane addition to actin remodeling at the invaginating metaphase furrow, which may also be true for conventional cytokinesis. Further, because membrane addition requires transient actin depolymerization (Eitzen, 2003), by promoting actin polymerization at the site of membrane addition, this pathway compensates for the transient loss of F-actin during vesicle delivery.

Materials and methods

Fly strains and genetics

Experiments involving all *nuf* or *Rab11* mutants were performed using the nuf^{1}-null allele or $Rab11^{i2D1}/Rab11^{93Bi}$ transheterozygous combination (Rothwell et al., 1998, 1999; Riggs et al., 2003). Germline clones of $RhoGEF2^{4.1}$ were generated using the FLP-DFS technique (Chou and Perrimon, 1996). The following stocks were obtained from the Bloomington Drosophila Stock Center (Indiana) and are reported as null (N) or hypomorphic alleles (H) according to Flybase: $Rab11^{i2D1}$ (H), $Rab11^{93Bi}$ (H), $RhoGEF2^{4.1}$ (N), $Rho1^{72O}$ (N), dia^{5} (N), $chic^{221}$ (N), $Sop2^{Q25sd}$ (N), tsr^{1} (H), tsr^{N96A} (N), and tsr^{N121} (N). For live embryo imaging, we used the following stocks: GFP-Moesin (gift from D. Kiehart, Duke University, Durham, NC; Edwards et al., 1997), GFP-Dlg (FlyTrap Project; Quinones-Coello et al., 2007), and Spider-GFP (created by A. Debec, Université Pierre et Marie Curie, Observatoire Océanologique, Villefranche-sur-mer, France), provided by J. Lippincott-Schwartz (National Institutes of Health, Bethesda, MD). Oregon R flies served as the WT control for all immunostained samples. All stocks were raised at 25°C on standard maize meal/molasses media.

Embryo fixation and immunostaining

Embryos were dechorionated in 50% Clorox bleach solution pretreated with 1:1 PBS/heptane solution for 45 s before adding an equal volume of 16.5% formaldehyde + 18% PFA (EM Sciences). The embryos were fixed for 22–25 min at 25°C and devitellinized by hand with a needle under a dissecting microscope. Immunofluorescence analysis was performed as previously described (Rothwell and Sullivan, 2000; Sisson et al., 2000). Alexa 488–conjugated, Rhodamine-conjugated, or Alexa 647–conjugated phalloidin (Invitrogen) was used to stain F-actin, and propidium iodide was used to stain DNA. The primary antibodies used include the following: rabbit anti-RhoGEF2 (1:500; provided by S. Rogers, University of North Carolina, Chapel Hill, NC; Rogers et al., 2004), mouse anti-Rho1 (1:10; Developmental Studies Hybridoma Bank), rabbit anti-Diaphanous (1:1,000; provided by S. Wasserman, University of California, San Diego, La Jolla, CA; Afshar et al., 2000), mouse anti-Dlg (1:100; provided by C. Doe, University of Oregon, Eugene, OR; Zito et al., 1997), and Cy5-conjugated anti-Anillin (1:200; Field and Alberts, 1995). Secondary Alexa 488–conjugated antibodies were used at 1:300 (Invitrogen).

Live embryo analysis

Embryos were prepared for microinjection and time-lapse scanning confocal microscopy as previously described (Tram et al., 2001). Except in Figs. 6 C and S4 C, all the reagents were injected at the 50% egg length and were diluted ~100-fold in the embryos (Foe and Alberts, 1983). Except for the experiment after actin incorporation into the furrow, 10 mg/ml Rhodamine-conjugated actin (Cytoskeleton, Inc.) and 10 mg/ml Rhodamine-conjugated tubulin (Cytoskeleton, Inc.) were injected into the embryos one cycle before drug injections and imaging. The following drugs were injected either at early cycle-13 prophase or early cellularization: DMSO alone (Sigma-Aldrich), 2 mM Latrunculin A (in DMSO; Sigma-Aldrich), 1 mM Jasp (in DMSO; EMD and provided by P. Crews, University of California, Santa Cruz, Santa Cruz, CA), and 1 mg/ml C3 exotransferase (Cytoskeleton, Inc.). C3 transferase is an ADP ribosyl transferase that selectively ribosylates and inactivates Rho-GTP with high specificity (Aktories et al., 1989; Sekine et al., 1989). 1 mg/ml of the constitutively active form of human recombinant RhoA protein (Q63L; Cytoskeleton Inc.) was injected at either early cycle-13 interphase or early cellularization. RhoA(Q63L) has a glutamine-to-leucine substitution at residue 63, preventing GTP hydrolysis, and maintains the protein in the active GTP-bound state (Gallo et al., 2002; Zhang et al., 2003). As described previously (Sisson et al., 2000), DMSO injection alone caused nuclei to move slightly away from the embryo cortex, but it had little effect on membrane and actin dynamics at the furrow.

Confocal microscopy, image quantifications, and statistics

Confocal microscope images were captured on an inverted photoscope (DMIRB; Leitz) equipped with a laser confocal imaging system (TCS SP2;

Leica) using an HCX PL APO 1.4 NA 63× oil objective (Leica) at room temperature. Except in FRAP experiments, ImageJ software (National Institutes of Health) was used to quantify the confocal images. For LatA injection experiments (Fig. 1 B), fluorescence intensities of GFP-Moesin and Rhodamine-actin at the furrows were subtracted from the background intensities measured from the nucleus regions. At least eight furrows and eight nuclear regions were analyzed in each embryo. In Table I and Fig. 7 G, based on the furrow morphology, embryos were classified into different groups: weak furrow (>10% of the furrows within an embryo showing uneven F-actin distribution), very weak furrow (>10% of the furrows within an embryo showing very uneven F-actin distribution), with breaks in furrow (>5% of the furrows within an embryo are broken), and normal furrow morphology. Student's *t* test (two-tailed, equal variance) was performed to analyze the data for furrow invagination, furrow-break index, and spindle-fusion index. Error bars represent the SEM from at least three independent experiments. For videos, image series collected over time were cropped in ImageReady (v9.0; Adobe) and converted to QuickTime (Apple) videos using PNG lossless compression.

FRAP analysis

Imaging was controlled by the Leica Confocal Software Microlab. After five prebleach scans of an entire image, 10 bleaching scans (0.7 s each) with 100% intensity of 488 nm (for GFP-Moesin) or 100% intensity of 488 and 543 nm (for Rhodamine-labeled actin) over the region of interest (10 × 10 µm) were performed. After photobleaching, the fluorescence recovery was monitored 10 times every 0.7 s and 60 times every 2 s. The recovery of fluorescence intensities, specifically at the furrow regions, was measured with Microlab. This software only measures a fixed x-y region. Thus, in a few cases where furrow structures showed slight drifts during fluorescence recovery, the FRAP image series were quantified using ImageJ software. The intensity of the bleached furrow area was normalized to the background nonbleached area. Recovery percentage was calculated as the final plateau intensity (I_F) minus the first intensity after photobleaching (I_0) all divided by the difference between prebleach (I_I) and postbleach (I_0) intensities ($[I_F - I_0]/[I_I - I_0]$). The fluorescence intensity of each time-point (I_t) was transformed into a 0–1 scale calculated by $[I_t - I_0]/[I_I - I_0]$. The values of relative intensities versus time were plotted using Excel (2004; Microsoft), and the recovery $t_{1/2}$ was measured from the plots.

Online supplemental material

Fig. S1 shows that GFP-Moesin marks F-actin cap and furrow. Fig. S2 shows that Jasp induces excess actin polymerization around the furrow. Fig. S3 shows that LatA injection results in disruption of GFP-Dlg and Spider-GFP–marked furrow plasma membrane integrity. Fig. S4 shows suppression of *nuf* phenotypes. Fig. S5 shows localization of RhoGEF2 and F-actin in *nuf* and *Rab11* embryos. Video 1 shows that F-actin signal is rapidly recovered at the furrow after photobleaching. Video 2 shows that LatA injection results in loss of membrane integrity and spindle fusions. Video 3 shows that F-actin is not stably maintained in *nuf* embryos. Video 4 shows that F-actin loss precedes membrane loss in *nuf* embryos. Video 5 shows that reducing the dosage of Twinstar stabilizes F-actin at the furrow in *nuf* embryos. Video 6 shows that GFP-Dlg–marked furrow membrane is not stably maintained in *nuf* embryos treated with DMSO. Video 7 shows that Jasp injection stabilizes membrane at the furrow in *nuf* embryos. Video 8 shows that C3 exotransferase injection results in loss of membrane integrity and spindle fusions. Video 9 shows that RhoA(Q63L) suppresses the *nuf* furrow defects local to the injection site. Online supplemental material is available at http://www.jcb.org/cgi/content/full/jcb.200712036/DC1.

We thank A. Debec, J. Lippincott-Schwartz, S. Rogers, S. Wasserman, C. Doe, and P. Crews for generously providing fly stocks, antibodies, and Jasp. We also thank L. Serbus, A. Royou, C. Lindley, and J. Crest for manuscript comments.

This work was supported by National Institutes of Health grant to W. Sullivan (GM046409), National Institutes of Health postdoctoral fellowship to R. Albertson (GM075670), and National Institutes of Health grant to C. Field (GM 58903).

Submitted: 10 December 2007
Accepted: 24 June 2008

References

Afshar, K., B. Stuart, and S.A. Wasserman. 2000. Functional analysis of the *Drosophila* diaphanous FH protein in early embryonic development. *Development.* 127:1887–1897.

Aktories, K., U. Braun, S. Rosener, I. Just, and A. Hall. 1989. The rho gene product expressed in *E. coli* is a substrate of botulinum ADP-ribosyltransferase C3. *Biochem. Biophys. Res. Commun.* 158:209–213.

Albertson, R., B. Riggs, and W. Sullivan. 2005. Membrane traffic: a driving force in cytokinesis. *Trends Cell Biol.* 15:92–101.

Bement, W.M., H.A. Benink, and G. von Dassow. 2005. A microtubule-dependent zone of active RhoA during cleavage plane specification. *J. Cell Biol.* 170:91–101.

Bubb, M.R., I. Spector, B.B. Beyer, and K.M. Fosen. 2000. Effects of jasplakinolide on the kinetics of actin polymerization. An explanation for certain in vivo observations. *J. Biol. Chem.* 275:5163–5170.

Cao, L.G., and Y.L. Wang. 1990. Mechanism of the formation of contractile ring in dividing cultured animal cells. I. Recruitment of preexisting actin filaments into the cleavage furrow. *J. Cell Biol.* 110:1089–1095.

Castrillon, D.H., and S.A. Wasserman. 1994. Diaphanous is required for cytokinesis in *Drosophila* and shares domains of similarity with the products of the limb deformity gene. *Development.* 120:3367–3377.

Chang, F., D. Drubin, and P. Nurse. 1997. cdc12p, a protein required for cytokinesis in fission yeast, is a component of the cell division ring and interacts with profilin. *J. Cell Biol.* 137:169–182.

Chou, T.B., and N. Perrimon. 1996. The autosomal FLP-DFS technique for generating germline mosaics in *Drosophila melanogaster*. *Genetics.* 144:1673–1679.

Crawford, J.M., N. Harden, T. Leung, L. Lim, and D.P. Kiehart. 1998. Cellularization in *Drosophila melanogaster* is disrupted by the inhibition of rho activity and the activation of Cdc42 function. *Dev. Biol.* 204:151–164.

D'Avino, P.P., M.S. Savoian, and D.M. Glover. 2005. Cleavage furrow formation and ingression during animal cytokinesis: a microtubule legacy. *J. Cell Sci.* 118:1549–1558.

Echard, A., G.R. Hickson, E. Foley, and P.H. O'Farrell. 2004. Terminal cytokinesis events uncovered after an RNAi screen. *Curr. Biol.* 14:1685–1693.

Edwards, K.A., M. Demsky, R.A. Montague, N. Weymouth, and D.P. Kiehart. 1997. GFP-moesin illuminates actin cytoskeleton dynamics in living tissue and demonstrates cell shape changes during morphogenesis in *Drosophila*. *Dev. Biol.* 191:103–117.

Eggert, U.S., A.A. Kiger, C. Richter, Z.E. Perlman, N. Perrimon, T.J. Mitchison, and C.M. Field. 2004. Parallel chemical genetic and genome-wide RNAi screens identify cytokinesis inhibitors and targets. *PLoS Biol.* 2:e379.

Eitzen, G. 2003. Actin remodeling to facilitate membrane fusion. *Biochim. Biophys. Acta.* 1641:175–181.

Emery, G., A. Hutterer, D. Berdnik, B. Mayer, F. Wirtz-Peitz, M.G. Gaitan, and J.A. Knoblich. 2005. Asymmetric Rab 11 endosomes regulate delta recycling and specify cell fate in the *Drosophila* nervous system. *Cell.* 122:763–773.

Farkas, R.M., M.G. Giansanti, M. Gatti, and M.T. Fuller. 2003. The *Drosophila* Cog5 homologue is required for cytokinesis, cell elongation, and assembly of specialized Golgi architecture during spermatogenesis. *Mol. Biol. Cell.* 14:190–200.

Field, C.M., and B.M. Alberts. 1995. Anillin, a contractile ring protein that cycles from the nucleus to the cell cortex. *J. Cell Biol.* 131:165–178.

Field, C.M., M. Coughlin, S. Doberstein, T. Marty, and W. Sullivan. 2005. Characterization of anillin mutants reveals essential roles in septin localization and plasma membrane integrity. *Development.* 132:2849–2860.

Fielding, A.B., E. Schonteich, J. Matheson, G. Wilson, X. Yu, G.R. Hickson, S. Srivastava, S.A. Baldwin, R. Prekeris, and G.W. Gould. 2005. Rab11-FIP3 and FIP4 interact with Arf6 and the exocyst to control membrane traffic in cytokinesis. *EMBO J.* 24:3389–3399.

Foe, V.E., and B.M. Alberts. 1983. Studies of nuclear and cytoplasmic behaviour during the five mitotic cycles that precede gastrulation in *Drosophila* embryogenesis. *J. Cell Sci.* 61:31–70.

Foe, V.E., G.M. Odell, and B.A. Edgar. 1993. Mitosis and morphogenesis in the *Drosophila* embryo: point and counterpoint. *In* The Development of *Drosophila melanogaster*. M. Bate and A. Martinez-Arias, editors. Cold Spring Harbor Laboratory Press, Cold Spring Harbor, NY. 149–300.

Foe, V.E., C.M. Field, and G.M. Odell. 2000. Microtubules and mitotic cycle phase modulate spatiotemporal distributions of F-actin and myosin II in *Drosophila* syncytial blastoderm embryos. *Development.* 127: 1767–1787.

Frescas, D., M. Mavrakis, H. Lorenz, R. Delotto, and J. Lippincott-Schwartz. 2006. The secretory membrane system in the *Drosophila* syncytial blastoderm embryo exists as functionally compartmentalized units around individual nuclei. *J. Cell Biol.* 173:219–230.

Gallo, G., H.F. Yee Jr., and P.C. Letourneau. 2002. Actin turnover is required to prevent axon retraction driven by endogenous actomyosin contractility. *J. Cell Biol.* 158:1219–1228.

Giansanti, M.G., G. Belloni, and M. Gatti. 2007. Rab11 is required for membrane trafficking and actomyosin ring constriction in meiotic cytokinesis of *Drosophila* males. *Mol. Biol. Cell.* 18:5034–5037.

Giansanti, M.G., S. Bonaccorsi, B. Williams, E.V. Williams, C. Santolamazza, M.L. Goldberg, and M. Gatti. 1998. Cooperative interactions between the central spindle and the contractile ring during *Drosophila* cytokinesis. *Genes Dev.* 12:396–410.

Glotzer, M. 2005. The molecular requirements for cytokinesis. *Science.* 307:1735–1739.

Gregory, S.L., T. Shandala, L. O'Keefe, L. Jones, M.J. Murray, and R. Saint. 2007. A *Drosophila* overexpression screen for modifiers of Rho signalling in cytokinesis. *Fly.* 1:13–22.

Grosshans, J., C. Wenzl, H.M. Herz, S. Bartoszewski, F. Schnorrer, N. Vogt, H. Schwarz, and H.A. Muller. 2005. RhoGEF2 and the formin Dia control the formation of the furrow canal by directed actin assembly during *Drosophila* cellularisation. *Development.* 132:1009–1020.

Guha, M., M. Zhou, and Y.L. Wang. 2005. Cortical actin turnover during cytokinesis requires myosin II. *Curr. Biol.* 15:732–736.

Gunsalus, K.C., S. Bonaccorsi, E. Williams, F. Verni, M. Gatti, and M.L. Goldberg. 1995. Mutations in *twinstar*, a *Drosophila* gene encoding a cofilin/ADF homologue, result in defects in centrosome migration and cytokinesis. *J. Cell Biol.* 131:1243–1259.

Harden, N., M. Ricos, Y.M. Ong, W. Chia, and L. Lim. 1999. Participation of small GTPases in dorsal closure of the *Drosophila* embryo: distinct roles for Rho subfamily proteins in epithelial morphogenesis. *J. Cell Sci.* 112:273–284.

Hariharan, I.K., K.Q. Hu, H. Asha, A. Quintanilla, R.M. Ezzell, and J. Settleman. 1995. Characterization of rho GTPase family homologues in *Drosophila melanogaster*: overexpressing Rho1 in retinal cells causes a late developmental defect. *EMBO J.* 14:292–302.

Hickson, G.R., J. Matheson, B. Riggs, V.H. Maier, A.B. Fielding, R. Prekeris, W. Sullivan, F.A. Barr, and G.W. Gould. 2003. Arfophilins are dual Arf/Rab 11 binding proteins that regulate recycling endosome distribution and are related to *Drosophila* nuclear fallout. *Mol. Biol. Cell.* 14:2908–2920.

Horgan, C.P., A. Oleksy, A.V. Zhdanov, P.Y. Lall, I.J. White, A.R. Khan, C.E. Futter, J.G. McCaffrey, and M.W. McCaffrey. 2007. Rab11-FIP3 is critical for the structural integrity of the endosomal recycling compartment. *Traffic.* 8:414–430.

Hudson, A.M., and L. Cooley. 2002. A subset of dynamic actin rearrangements in *Drosophila* requires the Arp2/3 complex. *J. Cell Biol.* 156:677–687.

Lecuit, T., and E. Wieschaus. 2000. Polarized insertion of new membrane from a cytoplasmic reservoir during cleavage of the *Drosophila* embryo. *J. Cell Biol.* 150:849–860.

Lee, O.K., K.K. Frese, J.S. James, D. Chadda, Z.H. Chen, R.T. Javier, and K.O. Cho. 2003. Discs-Large and Strabismus are functionally linked to plasma membrane formation. *Nat. Cell Biol.* 5:987–993.

Maxfield, F.R., and T.E. McGraw. 2004. Endocytic recycling. *Nat. Rev. Mol. Cell Biol.* 5:121–132.

Mukhina, S., Y.L. Wang, and M. Murata-Hori. 2007. Alpha-actinin is required for tightly regulated remodeling of the actin cortical network during cytokinesis. *Dev. Cell.* 13:554–565.

Murthy, K., and P. Wadsworth. 2005. Myosin-II-dependent localization and dynamics of F-actin during cytokinesis. *Curr. Biol.* 15:724–731.

Ng, J., and L. Luo. 2004. Rho GTPases regulate axon growth through convergent and divergent signaling pathways. *Neuron.* 44:779–793.

O'Connell, C.B., A.K. Warner, and Y. Wang. 2001. Distinct roles of the equatorial and polar cortices in the cleavage of adherent cells. *Curr. Biol.* 11:702–707.

Ono, S. 2007. Mechanism of depolymerization and severing of actin filaments and its significance in cytoskeletal dynamics. *Int. Rev. Cytol.* 258:1–82.

Padash Barmchi, M., S. Rogers, and U. Hacker. 2005. *DRhoGEF2* regulates actin organization and contractility in the *Drosophila* blastoderm embryo. *J. Cell Biol.* 168:575–585.

Pelham, R.J., and F. Chang. 2002. Actin dynamics in the contractile ring during cytokinesis in fission yeast. *Nature.* 419:82–86.

Pelissier, A., J.P. Chauvin, and T. Lecuit. 2003. Trafficking through Rab11 endosomes is required for cellularization during *Drosophila* embryogenesis. *Curr. Biol.* 13:1848–1857.

Piekny, A., M. Werner, and M. Glotzer. 2005. Cytokinesis: welcome to the Rho zone. *Trends Cell Biol.* 15:651–658.

Prokopenko, S.N., A. Brumby, L. O'Keefe, L. Prior, Y. He, R. Saint, and H.J. Bellen. 1999. A putative exchange factor for Rho1 GTPase is required for initiation of cytokinesis in *Drosophila*. *Genes Dev.* 13:2301–2314.

Quinones-Coello, A.T., L.N. Petrella, K. Ayers, A. Melillo, S. Mazzalupo, A.M. Hudson, S. Wang, C. Castiblanco, M. Buszczak, R.A. Hoskins, and L. Cooley. 2007. Exploring strategies for protein trapping in *Drosophila*. *Genetics.* 175:1089–1104.

Riggs, B., B. Fasulo, A. Royou, S. Mische, J. Cao, T.S. Hays, and W. Sullivan. 2007. The concentration of Nuf, a Rab11 effector, at the microtubule-organizing center is cell cycle regulated, dynein-dependent, and coincides with furrow formation. *Mol. Biol. Cell.* 18:3313–3322.

Riggs, B., W. Rothwell, S. Mische, G.R. Hickson, J. Matheson, T.S. Hays, G.W. Gould, and W. Sullivan. 2003. Actin cytoskeleton remodeling during early *Drosophila* furrow formation requires recycling endosomal components Nuclear-fallout and Rab11. *J. Cell Biol.* 163:143–154.

Rogers, S.L., U. Wiedemann, U. Hacker, C. Turck, and R.D. Vale. 2004. *Drosophila* RhoGEF2 associates with microtubule plus ends in an EB1-dependent manner. *Curr. Biol.* 14:1827–1833.

Rothwell, W.F., and W. Sullivan. 2000. Fluorescent analysis of *Drosophila* embryos. *In* Drosophila Protocols. W. Sullivan, M. Ashburner, and R.S. Hawley, editors. Cold Spring Harbor Laboratory Press, Cold Spring Harbor, NY. 141–157.

Rothwell, W.F., P. Fogarty, C.M. Field, and W. Sullivan. 1998. Nuclear-fallout, a *Drosophila* protein that cycles from the cytoplasm to the centrosomes, regulates cortical microfilament organization. *Development.* 125:1295–1303.

Rothwell, W.F., C.X. Zhang, C. Zelano, T.S. Hsieh, and W. Sullivan. 1999. The *Drosophila* centrosomal protein Nuf is required for recruiting Dah, a membrane associated protein, to furrows in the early embryo. *J. Cell Sci.* 112:2885–2893.

Royou, A., C. Field, J.C. Sisson, W. Sullivan, and R. Karess. 2004. Reassessing the role and dynamics of nonmuscle myosin II during furrow formation in early *Drosophila* embryos. *Mol. Biol. Cell.* 15:838–850.

Schroeder, T.E. 1972. The contractile ring. II. Determining its brief existence, volumetric changes, and vital role in cleaving *Arbacia* eggs. *J. Cell Biol.* 53:419–434.

Sekine, A., M. Fujiwara, and S. Narumiya. 1989. Asparagine residue in the Rho gene product is the modification site for botulinum ADP-ribosyltransferase. *J. Biol. Chem.* 264:8602–8605.

Sisson, J.C., C. Field, R. Ventura, A. Royou, and W. Sullivan. 2000. Lava lamp, a novel peripheral Golgi protein, is required for *Drosophila melanogaster* cellularization. *J. Cell Biol.* 151:905–918.

Skop, A.R., D. Bergmann, W.A. Mohler, and J.G. White. 2001. Completion of cytokinesis in *C. elegans* requires a brefeldin A-sensitive membrane accumulation at the cleavage furrow apex. *Curr. Biol.* 11:735–746.

Skop, A.R., H. Liu, J. Yates III, B.J. Meyer, and R. Heald. 2004. Dissection of the mammalian midbody proteome reveals conserved cytokinesis mechanisms. *Science.* 305:61–66.

Somma, M.P., B. Fasulo, G. Cenci, E. Cundari, and M. Gatti. 2002. Molecular dissection of cytokinesis by RNA interference in *Drosophila* cultured cells. *Mol. Biol. Cell.* 13:2448–2460.

Stevenson, V., A. Hudson, L. Cooley, and W.E. Theurkauf. 2002. Arp2/3-dependent pseudocleavage [correction of psuedocleavage] furrow assembly in syncytial *Drosophila* embryos. *Curr. Biol.* 12:705–711.

Sullivan, W., P. Fogarty, and W. Theurkauf. 1993. Mutations affecting the cytoskeletal organization of syncytial *Drosophila* embryos. *Development.* 118:1245–1254.

Tram, U., B. Riggs, C. Koyama, A. Debec, and W. Sullivan. 2001. Methods for the study of centrosomes in *Drosophila* during embryogenesis. *Methods Cell Biol.* 67:113–123.

Ullrich, O., S. Reinsch, S. Urbe, M. Zerial, and R.G. Parton. 1996. Rab11 regulates recycling through the pericentriolar recycling endosome. *J. Cell Biol.* 135:913–924.

Wilson, G.M., A.B. Fielding, G.C. Simon, X. Yu, P.D. Andrews, R.S. Hames, A.M. Frey, A.A. Peden, G.W. Gould, and R. Prekeris. 2005. The FIP3-Rab11 protein complex regulates recycling endosome targeting to the cleavage furrow during late cytokinesis. *Mol. Biol. Cell.* 16:849–860.

Xu, H., J.A. Brill, J. Hsien, R. McBride, G.L. Boulianne, and W.S. Trimble. 2002. Syntaxin 5 is required for cytokinesis and spermatid differentiation in *Drosophila*. *Dev. Biol.* 251:294–306.

Zhang, X.F., A.W. Schaefer, D.T. Burnette, V.T. Schoonderwoert, and P. Forscher. 2003. Rho-dependent contractile responses in the neuronal growth cone are independent of classical peripheral retrograde actin flow. *Neuron.* 40:931–944.

Zito, K., R.D. Fetter, C.S. Goodman, and E.Y. Isacoff. 1997. Synaptic clustering of Fascilin II and Shaker: essential targeting sequences and role of Dlg. *Neuron.* 19:1007–1016.